International Journal of Steel Structures
December 2014, Vol 14, No 4, 797-810
DOI 10.1007/s13296-014-1211-1

International Journal of
STEEL
STRUCTURES
www.springer.com/journal/13296

Dynamic Responses of a Continuous Beam Railway Bridge under Moving High Speed Train with Random Track Irregularity

Di Mu[1] and Dong-Ho Choi[2,*]

[1]*Ph.D. Candidate, Department of Civil and Environmental Engineering, Hanyang University, Seoul, 133-791, Korea*
[2]*Professor, Department of Civil and Environmental Engineering, Hanyang University, Seoul, 133-791, Korea*

Abstract

This paper addresses the dynamic response of a continuous beam bridge with different levels of track irregularities under a single, moving high-speed train. The train is modeled as one-foot sprung masses. The bridge is described as an Euler-Bernoulli beam supported by several hinged supports. Rayleigh damping coefficients of the bridge are calculated by using the modal damping ratio. Random track irregularities are generated by power spectrum density functions. The interaction equation of motion is derived and then solved by using the Newmark-beta method combined with the Newton-Raphson method. The dynamic impact factors of a single-span simply supported bridge and a five-span continuous beam bridge under the same train are calculated and compared for verification. Additionally, a three-span continuous beam bridge with various damping ratios and track irregularities under a Korea Train Express (KTX) train is used as an example to investigate the dynamic impact factors at the midpoints of different bridge spans in both downward and upward directions, the deck rotations at the bridge supports, and the average maximum acceleration of the train bodies under different conditions.

Keywords: continuous beam bridge, random track irregularities, different span responses, moving trainload, time-incremental analysis

1. Introduction

In recent decades, train operating speeds have been greatly enhanced, and many new high-speed railway lines have been built. However, a lack of preliminary dynamic analysis in the bridge design procedure may lead to various problems during operation, especially for normal or short span continuous beam bridges, owing to the naturally high frequencies of bridges. For bridges, trainload is a type of heavy periodic load. Resonance between the train and bridge may lead to vibrations over the limits for the bridge and train. Large and unexpected bridge vibrations cause structural damage to the bridge, intensifying the rail wear and reducing the driving comfort of the train. Thus, a relatively fast and accurate estimation of bridge and vehicle vibration can provide necessary data for engineers to adjust their designs or choose the effective way to strengthen the existing bridges.

Note.-Discussion open until May 1, 2015. This manuscript for this paper was submitted for review and possible publication on March 10, 2014; approved on December 1, 2014.

*Corresponding author
Tel: +82-2-2220-0328; Fax: +82-2-2220-4322
E-mail: samga@hanyang.ac.kr

There are two main ways to analyze bridge vibration problems: analytical and numerical. In early studies, researchers used concentrated forces or uniform distributed forces to model trainloads. This type of model only considers the train gravity and can determine the analytical solution for bridge vibration. Thambiratnam and Zhuge (1996) analyzed the dynamic behavior of a beam with variable thickness on an elastic foundation subjected to a moving concentrated force. Yang *et al.* (1997) and Fryba (2001) modeled a train as a series of concentrated forces and discussed the effects of bridge span length and resonance behavior. Lacarbonara and Colone (2007) applied this model to an arch bridge. The moving force model can maintain sufficient accuracy when the train mass is relatively small compared to the bridge mass, but in realistic conditions, the train mass is large enough to cause significant geometric nonlinearity to the system. To consider the inertia of the train, the lumped mass model was developed. Akin and Mofid (1989) and Dehestani *et al.* (2009) used the modal superposition method to derive the analytical-numerical solution for a moving mass on an Euler beam and discussed the influence of mass moving speeds. Wang (1998) investigated a finite inextensible beam on an elastic foundation under an accelerating mass. However, this model ignored the cushioning ability of train suspension systems; thus, the calculated vibration

responses were larger than the real conditions. To solve this problem, the train was modeled as a series of lumped masses supported by springs, also called the sprung mass model. In this model, there is no direct contact between train masses and the bridge. Lu *et al*. (2012), Mao and Lu (2013), and Mazilu (2013) used this model to determine a closed-form solution for bridge vibration. To consider the direct contact between wheel sets and rail, the one-foot moving sprung mass model was developed. This model divided the car into several individual parts, usually located at the centers of the bogies or wheel sets. Yang and Lin (1995) studied the interaction between one-foot sprung masses and bridges and discussed the impact effects with different train speeds. Yang and Yau (1997) added ballast stiffness into the train-bridge model and performed an incremental dynamic analysis, solved with iteration steps. The one-foot sprung mass model can provide more accurate results for both bridge and train responses.

The Euler-Bernoulli beam model is the most widely used model of bridges because it can conveniently generate both analytical and numerical solutions. For representing the vertical vibration of slender bridge structures, the two-dimensional Euler-Bernoulli beam model can provide satisfactory results. Most studies on bridge vibration use the one-span simply supported bridge model as a sample of practical multi-span simply supported bridges. Chu *et al*. (1986) studied the dynamic impact of one-span prestressed concrete bridges with track irregularities. Nikkhoo *et al*. (2007) developed a modal control algorithm for the moving mass problem. Majka and Hartnett (2008) discussed the effects of train speed, mass, and damping ratio. Wu and Yang (2003) expanded the single-span simply supported bridge model to multispan simply supported bridges to determine the steady-state response of the bridge. The continuous beam bridge is a popular railway bridge type, particularly the prestressed concrete continuous beam bridge. The dynamic responses of this type of bridge are slightly different from those of simply supported beam bridges. Olsson (1985) studied a two-span plate girder model with surface irregularities and different train models. Another study on two-span continuous bridges is that of Shin *et al*. (2010), who used the moving force model and discussed adding special length cars to the normal train to reduce the resonance. Kwark *et al*. (2004) analyzed a two-span KHST railway bridge vibration and verified the analysis with a field test. Stancioiu *et al*. (2011) experimentally studied a four-span continuous flexible structure subjected to moving mass and compared the result with the theoretical solution. Recently, Johansson *et al*. (2013) used the concentrated force model and modal superposition method to determine the analytical solution for multispan beam bridges. However, studies on continuous bridges with three different spans and various levels of track irregularities under a moving train have not been performed in detail.

This paper describes the one-foot moving sprung mass model of a train with a continuous beam bridge as an Euler beam supported by several hinged or rolling supports. The bridge Rayleigh damping coefficients are calculated from the modal damping ratio and natural frequencies of the bridge. Vertical, random track irregularities are generated based on the empirical power spectrum density (PSD) formula. The responses of bridge, train, and wheel with different levels of track irregularities and damping ratio are investigated. To investigate the response of the continuous beam bridge, a three-span continuous beam bridge with various damping ratios and track irregularities under a KTX train is taken as an example. The dynamic impact factor at midpoints of different bridge spans in both downward and upward directions, the deck rotations at the bridge supports, and the average maximum acceleration of the train bodies are calculated and discussed.

2. Model of the Train

The planar train model with N_v numbers of one-foot sprung masses is shown in Fig. 1. Each car is divided into four one-foot sprung masses located at the positions of the wheel sets. Each one-foot sprung mass has two vertical degrees of freedom, u_w and u_v, which represent the displacements of the wheel and the car body, respectively. For the jth one-foot sprung mass, the upper mass, m_{vj}, represents a quarter of the car body and half of the front or rear bogie; the lower mass, m_{wj}, represents the wheel set; the suspension system connecting these masses has stiffness k_{tj} and viscosity c_{tj}. The distance between the jth and j+1th one-foot sprung mass is L_j. Cheng *et al*. (2001) indicated that the contact force between the bridge and the lower mass is f_{cj}, which consists of a static element, f_{wj}, due to weight and a dynamic element, f_{dj}, due to vertical vibration, as shown below:

$$f_{cj} = f_{wj} + f_{dj} \tag{1}$$

$$f_{wj} = (m_{vj} + m_{wj})g \tag{2}$$

Initially, the train is in the vertical force equilibrium condition. Its dynamic equation of motion can be constructed as follows:

$$\begin{bmatrix} [M_{tw}] & [0] \\ [0] & [M_{tv}] \end{bmatrix} \begin{Bmatrix} \{\ddot{u}_w\} \\ \{\ddot{u}_v\} \end{Bmatrix} + \begin{bmatrix} [C_t] & -[C_t] \\ -[C_t] & [C_t] \end{bmatrix} \begin{Bmatrix} \{\dot{u}_w\} \\ \{\dot{u}_v\} \end{Bmatrix} + \begin{bmatrix} [k_v] & -[k_v] \\ -[k_v] & [k_v] \end{bmatrix} \begin{Bmatrix} \{u_w\} \\ \{u_v\} \end{Bmatrix} = \begin{Bmatrix} \{f_d\} \\ \{0\} \end{Bmatrix} \tag{3}$$

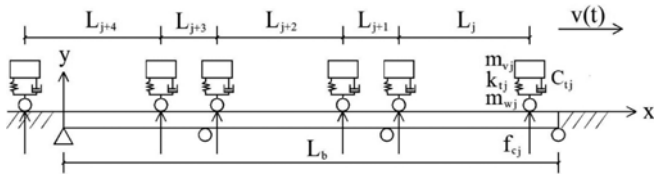

Figure 1. Model of the train and bridge.

3. Model of the bridge

Most high-speed railway bridges are simply supported box girder bridges or continuous beam bridges. These bridges can be modeled as two-dimensional homogeneous Euler beams, and the finite-element method can be used for analysis, as shown in Fig. 1. The beam is supported by hinges and rollers that stand for piers and abutments. The bridge is divided into N_m beam elements with same length, L, that are shorter than the minimum length between any one-foot sprung masses. In this case, at any time there will be, at most, one one-foot sprung mass on any beam element.

The linear density of the beam is $\overline{m}$, the stiffness modulus is E, and the second moment of inertia is I. The homogeneous beam element mass matrix, $[M_{be}]$, and stiffness matrix, $[K_{be}]$, are as follows:

$$[M_{be}] = \frac{\overline{m}L}{420}\begin{bmatrix} 156 & 22L & 54 & -13L \\ 22L & 4L^2 & 13L & -3L^2 \\ 54 & 13L & 156 & -22L \\ -13L & -3L^2 & -22L & 4L^2 \end{bmatrix} \quad (4)$$

$$[K_{be}] = \frac{EI}{L^3}\begin{bmatrix} 12 & 6L & -12 & 6L \\ 6L & 4L^2 & -6L & 2L^2 \\ -12 & -6L & 12 & -6L \\ 6L & 2L^2 & -6L & 4L^2 \end{bmatrix} \quad (5)$$

Bridge damping type is Rayleigh damping with the coefficients α and β, and the corresponding element damping matrix can be calculated as follows:

$$[C_{be}]=\alpha[M_{be}]+\beta[K_{be}] \quad (6)$$

The corresponding Rayleigh damping coefficients can be solved as:

$$\alpha = \zeta\frac{2\omega_1\omega_2}{\omega_1+\omega_2} \quad (7)$$

where ζ is the modal damping ratio, ω_1 and ω_2 are the first and second modal natural frequencies, respectively.

The bridge is initially in the static force equilibrium condition, so when the train approaches the bridge, the external loads acting on the bridge are contact forces, $-[N]\{f_c\}$, between wheel and bridge, where $[N]$ is the cubic Hermit interpolation matrix for the bridge elements with dynamic supporting force $\{p_s\}$ at the supports. The equation of motion of the whole bridge can be assembled as

$$[M_b]\{\ddot{u}_b\}+[C_b]\{\dot{u}_b\}+[K_b]\{u_b\} = -[N]\{f_c\}+\{p_s\} \quad (9)$$

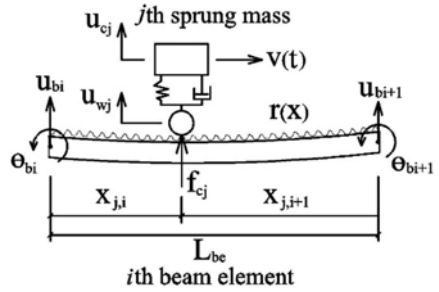

Figure 2. Definition sketch for the relative displacement between beam element and sprung mass.

4. Existing Function and Shape Constraints

The relation between the ith beam element and jth one-foot sprung mass is illustrated in Fig. 2. If the right end of a beam element is subject to counterclockwise rotation, the element will deflect in downward direction; meanwhile if the left end of a beam element is subject to counterclockwise rotation, the element will deflect in upward direction. To show the sprung mass existing on the beam element, the unit step function is included in the analysis:

$$H(x) = \begin{cases} 0 & x<0 \\ 1 & x\geq 0 \end{cases} \quad (10)$$

For the ith beam element from the left end of the bridge, its left node is located at $x_{il}=(i-1)L$, whereas its right node is located at $x_{ir}=iL$. At time t, the position of the jth one-foot sprung mass is located at x_j. Thus, the relative positions of the sprung mass to the left and right nodes of the beam element are $x_{j,i}=x_j-x_{il}$ and $x_{j,i+1}=x_j-x_{ir}$, respectively. Then the existing function for the jth one-foot sprung mass on the ith beam element is shown in Eq. (11). The $H_{j,i}$ only has a nonzero value when the one-foot sprung mass is on the beam element.

$$H_{j,i}=H(x_{j,i})-H(x_{j,i+1}) \quad (11)$$

The displacement relationship between the jth one-foot sprung mass and the ith beam element can be expressed

as a cubic Hermit vector $\{N_{j,i}\}$, as shown in Eq. (12). This vector links the beam nodal displacements and the vertical displacement of any point on the beam.

$$\{N_{j,i}\} = H_{j,i}\begin{Bmatrix} 1-3(x_{j,i}/L)^2+2(x_{j,i}/L)^3 \\ x_{j,i}[1-2(x_{j,i}/L)+(x_{j,i}/L)^2] \\ 3(x_{j,i}/L)^2-2(x_{j,i}/L)^3 \\ x_{j,i}[(x_{j,i}/L)-(x_{j,i}/L)] \end{Bmatrix} \tag{12}$$

For the jth one-foot sprung mass moving through the bridge, according to the sequence of beam nodes, the $\{N_{j,i}\}$ can be assembled into one vector, $\{N_j\}$, which shows the relationship between the bridge vertical displacement, u_j, at the position of the jth sprung mass and all beam elements nodal displacements:

$$u_j = \{N_j\}^T\{u_b\} \tag{13}$$

For the whole train, the interpolation vectors, $\{N_j\}$, can be assembled into a cubic Hermit interpolation matrix as in Eq. (14).

$$[N]=[\{N_1\}\{N_2\}\ \ldots\ \{N_{Nv}\}] \tag{14}$$

The track irregularities, $ir(x)$, and their time derivations at the positions of all one-foot sprung masses are

$$\{ir(x)\} = \langle ir(x_1)\ \ ir(x_2)\ \ \ldots\ \ ir(x_{Nv})\rangle^T \tag{15}$$

$$\frac{d\{ir(x)\}}{dt} = \frac{d\{ir(x)\}}{dx}\frac{dx}{dt} = [V]\{ir(x)\}_{,x} \tag{16}$$

$$\frac{d^2\{ir(x)\}}{dt^2} = \frac{d([V]\{ir(x)\}_{,x})}{dt} = [A_t]\{ir(x)\}_{,x}+[V]^2\{ir(x)\}_{,xx} \tag{17}$$

where $[V]$ and $[A_t]$ are the speed and acceleration of the one-foot sprung masses, respectively. Assuming that the wheel set is always in contact with the bridge, the vertical vibrations of wheel sets can be replaced by the bridge nodal displacements and track irregularities, as shown in Eq. (18) to (20).

$$\{u_w\} = [N]^T\{u_b\}+\{ir(x)\} \tag{18}$$

$$\{\dot{u}_w\} = [N]^T\{\dot{u}_b\}+[V][N]_{,x}^T\{u_b\}+[V]\{ir(x)\}_{,x} \tag{19}$$

$$\{\ddot{u}_w\} = [N]^T\{\ddot{u}_b\}+2[V][N]_{,x}^T\{\dot{u}_b\}+[A_t][N]_{,x}^T\{u_b\} +[V]^2[N]_{,x}^T\{u_b\}+[A_t]\{ir(x)\}_{,x}+[V]^2\{ir(x)\}_{,xx} \tag{20}$$

5. Random track irregularities

Track irregularities can cause large self-excitation within the train-bridge system, especially for high-speed railways. The characteristics of track irregularities are influenced by many factors; and for engineering requirements, they can be generated through the PSD function $S(\phi)$, where ϕ is the spatial frequency. According to the measured results of U.S. railway tracks, the PSD function for vertical track irregularity can be summarized as follows:

$$S(\phi) = \frac{A\phi_2^2(\phi^2+\phi_1^2)}{\phi^4(\phi^2+\phi^2)} \tag{21}$$

where the roughness coefficient, A, and the cutoff frequencies, ϕ_1 and ϕ_2, are determined based on measurements (Hamid and Yang, 1982). The values for different levels of tracks are listed in Table 1. The vertical irregularities are zero-mean stationary Gaussian random processes. Au *et al*. (2002) generated these irregularities by using a simple inverse Fourier transformation with a PSD function.

$$ir(x) = \sum_{k=1}^{N_k} a_k\cos(\phi_k x+\theta_k) \tag{22}$$

where the coefficient a_k is the wave amplitude, N_k is the amount of the cosine series, ϕ_k is the spatial frequency within the range $[\phi_{\min}\ \phi_{\max}]$, and θ_k is the random phase angle that varies between 0 and 2π. For the evaluation of a certain level track, choosing the corresponding A and defining $[\phi_{\min}\ \phi_{\max}]$ can produce the required level vertical track irregularities.

$$a_k = 2\sqrt{S(\phi_k)\Delta\phi} \tag{23}$$

$$\phi_k = \phi_{\min}+\left(k-\frac{1}{2}\right)\Delta\phi \tag{24}$$

$$\Delta\phi = (\phi_{\max}-\phi_{\min})/Nk \tag{25}$$

6. Coupling the Equation of Motion for a Train and a Bridge

The relationship of the equation of motion for a train and a bridge consists of the contact forces and shape constraints. The objective of coupling the equation is eliminating the vibrations of wheel sets, $\{u_w\}$, $\{\dot{u}_w\}$, and $\{\ddot{u}_w\}$. Substituting Eqs. (18)-(20) into Eq. (3) results in the expression of dynamic contact forces $\{f_d\}$:

Table 1. Coefficients in power spectrum density function

Track level	1	2	3	4	5	6
A (m^3/cycle)	15.563	8.865	4.925	2.758	1.556	0.887
ϕ_1 (cycle/s)	0.0233		ϕ_2 (cycle/s)		0.1312	

$$\{f_d\} = [M_{tw}][N]^T\{\ddot{u}_b\} + (2[M_{tw}][V][N]_{,x}^T + [C_t][N]^T)\{\dot{u}_b\} + ([M_{tw}][A_t][N]_{,x}^T + [M_{tw}][V]^2[N]_{,x}^T + [C_t][V][N]^T + [K_t][N]^T)\{u_b\} - [C_t]\{\dot{u}_v\} - [K_t]\{u_v\} + [M_{tw}][V]^2\{ir(x)\}_{,xx} + ([M_{tw}][A_t] + [C_t][V])\{ir(x)\}_{,x} + [K_t]\{ir(x)\} \quad (26)$$

Then, substituting the above equation and Eq. (3) into Eq. (9), and writing it into matrix form, the coupled equation of motion without the degrees of freedom of the wheels is generated:

$$\begin{bmatrix}[M_{11}] & [0]\\ [0] & [M_{22}]\end{bmatrix}\begin{Bmatrix}\{\ddot{u}_v\}\\ \{\ddot{u}_b\}\end{Bmatrix} + \begin{bmatrix}[C_{11}] & [C_{12}]\\ [C_{21}] & [C_{22}]\end{bmatrix}\begin{Bmatrix}\{\dot{u}_v\}\\ \{\dot{u}_b\}\end{Bmatrix} + \begin{bmatrix}[k_{11}] & [k_{12}]\\ [k_{21}] & [k_{22}]\end{bmatrix}\begin{Bmatrix}\{u_v\}\\ \{u_b\}\end{Bmatrix} = \begin{Bmatrix}\{P_v\}\\ \{P_b\}\end{Bmatrix} \quad (27)$$

where

$$[M_{11}] = [M_{tv}] \quad (28)$$

$$[M_{22}] = [M_b] + [N][M_{tv}][N]^T \quad (29)$$

$$[C_{11}] = [C_t] \quad (30)$$

$$[C_{12}] = -[C_t][N]^T \quad (31)$$

$$[C_{21}] = -[N][C_t] \quad (32)$$

$$[C_{22}] = [C_b] + 2[N][M_{tw}][V][N]_{,x}^T + [N][C_t][N]^T \quad (33)$$

$$[K_{11}] = [K_t] \quad (34)$$

$$[K_{12}] = -[C_t][V][N]_{,x}^T - [K_t][N]^T \quad (35)$$

$$[K_{21}] = -[N][K_t] \quad (36)$$

$$[K_{22}] = [K_b] + [N][M_{tw}][A_t][N]_{,x}^T + [N][V]^2[N]_{,xx}^T + [N][C_t][V][N]_{,x}^T + [N][K_t][N]^T \quad (37)$$

$$\{P_v\} = [C_t][V]\{ir(x)\}_{,x} + [K_t]\{ir(x)\} \quad (38)$$

$$\{P_b\} = -[N]\{f_w\} + [N][K_t]\{ir(x)\} + [N][C_t][V]\{ir(x)\}_{,x} + [N][M_{tw}][A_t]\{ir(x)\}_{,x} + [N][M_{tw}][V]^2\{ir(x)\}_{,xx} + \{p_s\} \quad (39)$$

7. Solution Procedures

Equation (27) can be solved through direct time integral methods such as the Newmark-β method or Wilson-θ method. Considering that its submatrices are almost time-dependent, this equation is nonlinear, and the Newton-Raphson iteration has to be applied in each time step to fix the errors. With both initial conditions of the bridge and train in vertical force equilibrium, the equation of motion is solved by average acceleration Newmark-β combined with the Newton-Raphson method by using the following steps. To easily express the equation of motion, the short form of Eq. (27) is written as Eq. (40).

$$[M]\{\ddot{U}\} + [C]\{\dot{U}\} + [K]\{U\} = \{P(t)\} \quad (40)$$

Step 1

At the beginning of each time step, update the time, speed of the train, $[V]$, position of each one-foot sprung mass, and relative positions, $x_{j,i}$. Judge the existing functions, $H_{j,i}$, and calculate the cubic Hermit interpolation matrix, $[N]$. Next, calculate the dynamic contact forces, $\{f_d\}$, and track irregularities, $\{ir(x)\}$.

Step 2

Assemble the mass matrix, $[M]$; damping matrix, $[C]$; and stiffness matrix, $[K]$. Update the external load, $\{P(t)\}$, and calculate the increment of external load by using Eq. (41).

$$\{\Delta P\} = \{P(t)\} - \{P(t-\Delta t)\} \quad (41)$$

The time increment form for Eq. (40) at time t is

$$[M]_t\{\Delta\ddot{U}\} + [C]_t\{\Delta\dot{U}\} + [K]_t\{\Delta U\} = \{\Delta P\} \quad (42)$$

Step 3

Rearrange Eq. (42) according to the free f and fixed r degrees of freedom. Subscripts and denote the free and restrained degrees of freedom, respectively.

$$\begin{bmatrix}[M_f] & [M_{fr}]\\ [M_{rf}] & [M_r]\end{bmatrix}\begin{Bmatrix}\{\Delta\ddot{U}_f\}\\ \{0\}\end{Bmatrix} + \begin{bmatrix}[C_f] & [C_{fr}]\\ [C_{rf}] & [C_x]\end{bmatrix}\begin{Bmatrix}\{\Delta\dot{U}_f\}\\ \{0\}\end{Bmatrix} + \begin{bmatrix}[K_f] & [K_{fr}]\\ [K_{rf}] & [K_r]\end{bmatrix}\begin{Bmatrix}\{\Delta U_f\}\\ \{0\}\end{Bmatrix} = \begin{Bmatrix}\{\Delta P_f\}\\ \{\Delta P_r\}\end{Bmatrix} \quad (43)$$

Step 4

Calculate the coefficient matrices in time increment calculation:

$$[A] = \frac{4}{\Delta t}[M_f] + 2[C_f] \quad (44)$$

$$[B] = 2[M_f] \tag{45}$$

The equivalent external load increment is

$$\{\Delta\hat{P}\} = \{\Delta P_f\} + [A]\{\dot{U}_f\} + [B]\{\ddot{U}_f\} \tag{46}$$

Determine the tangent stiffness matrix:

$$[\hat{K}] = [K_f] + \frac{2}{\Delta t}[C_f] + \frac{4}{(\Delta t)^2}[M_f] \tag{47}$$

Step 5

Start the modified Newton-Raphson iteration and determine the initial values from the present time step. The initial displacement vector and internal resisting force vector are

$$\{U_f(t+\Delta t)\}^{(0)} = \{U_f(t)\} \tag{48}$$

$$\{f_s\}^{(0)} = \{f_s(t)\} \tag{49}$$

The initial unbalanced force vector is

$$\{\Delta R\}^{(1)} = \{\Delta\hat{P}\} \tag{50}$$

Step 6

Start the modified Newton-Raphson iteration loops. For i=1, 2, 3, ..., calculate the incremental displacement vector.

$$\{\Delta u\}^{(i)} = [\hat{K}(t)]^{-1}\{\Delta R\}^{(i)} \tag{51}$$

If the incremental displacement vector is smaller than the given tolerance, terminate the current iteration step and go to next time step. If not, update the displacement vector:

$$\{U_f(t+\Delta t)\}^{(i)} = \{U_f(t+\Delta t)\}^{(i-1)} + \{\Delta u\}^{(i)} \tag{52}$$

Renew the internal resisting force vector and calculate the unbalanced force vector for next iteration:

$$\{\Delta R\}^{(i+1)} = \{\Delta R\}^{(i)} - [\{f_s\}^{(i)} - \{f_s\}^{(i-1)} + ([\hat{K}] - [K_f])\{\Delta u\}^{(i)}] \tag{53}$$

Step 7

Calculate the increments of speed and acceleration vectors:

$$\{\Delta\dot{u}\} = \frac{2}{\Delta t}\sum\{\Delta u\}^{(i)} - 2\{\dot{U}_f(t)\} \tag{54}$$

$$\{\Delta\dot{u}\} = \frac{4}{(\Delta t)^2}\sum\{\Delta u\}^{(i)} - \frac{4}{\Delta t}\{\dot{U}_f(t)\} - 2\{\ddot{U}_f(t)\} \tag{55}$$

Update the speed and acceleration vectors:

$$\{\dot{U}_f(t+\Delta t)\} = \{\dot{U}_f(t)\} + \{\Delta\dot{u}\} \tag{56}$$

$$\{\ddot{U}_f(t+\Delta t)\} = \{\ddot{U}_f(t)\} + \{\Delta\ddot{u}\} \tag{57}$$

8. Numerical Examples

In bridge structure design, the dynamic impact factor is very important for engineers to determine the allowable structural strength. This is described as the percentage difference between the dynamic response and the static response. The dynamic impact factor is usually evaluated at the critical point of the bridge, such as the midpoint of the span. The displacement dynamic factor is expressed in Eq. (58).

$$D_d = \frac{U_{d\max} - U_{s\max}}{U_{s\max}} \tag{58}$$

For dimensionless consideration, the speed ratio is defined as

$$\alpha = \frac{\pi}{\omega_b} \Big/ \frac{L}{v} \tag{59}$$

When α=1, the half fundamental period of the bridge is equal to the time taken by the first one-foot sprung mass to travel through the bridge.

8.1. Example 1: A simply supported bridge under a moving train with five cars

The properties of the bridge and train are described in Table 2. This example is widely used to verify the accuracy of the calculated result. The bridge has a constant cross section and the train is moving at a constant speed. The dynamic response is evaluated by the impact factor of the midpoint of the bridge versus different train speeds, as shown in Fig. 3. The result satisfactorily agrees with that found by Cheng *et al*. (2001).

8.2. Example 2: A five-span continuous bridge under a moving train with five cars

For verifying multispan bridges, a continuous bridge with five equal spans is considered. The train properties are the same as in Example 1. The piers are regarded as hinged supports. The properties of the bridge are described in Table 3. The bridge dynamic response, evaluated at the midpoint of the central span versus the different train speeds, is shown in Fig. 4. Compared to the result obtained by Cheung *et al*. (1999), satisfactory agreement is observed.

Comparing Fig. 4 with Fig. 3 indicates that although the properties of each bridge span and train are the same, the dynamic responses of the bridges are quite different. When the speed ratio $\alpha \subset [0 \;\; 0.35]$, the additional dynamic impacts for both bridge and train are small. There are two local resonance speed ratios: 0.12 and 0.17, for the simply supported bridge, and 0.12 and 0.2, for the continuous beam bridge. The impact of the simply supported bridge

Table 2. Bridge and train properties in Example 1

L_b (m)	$\overline{m}$ (kg/m)	I (m^4)	E (MPa)	N_m	ζ	
20	34088	3.81	29430	12	0%	
m_w (kg)	m_v (kg)	k_t (N/m)	c_t (Ns/m)	N_v	L_g (m)	L_c (m)
4400	17600	9.12×10^6	8.6×10^4	10	6	18

Table 3. Bridge properties in Example 2

L_b (m)	$\overline{m}$ (kg/m)	I (m^4)	E (MPa)	N_m	ζ
5@20	34088	3.81	29430	80	0%

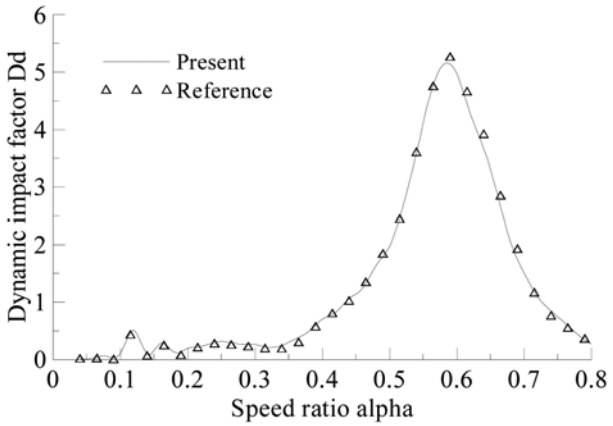

Figure 3. Dynamic impact factor at midpoint of simply supported bridge with a span of 20 m, 0% damping ratio, and no track irregularities under a train with five cars.

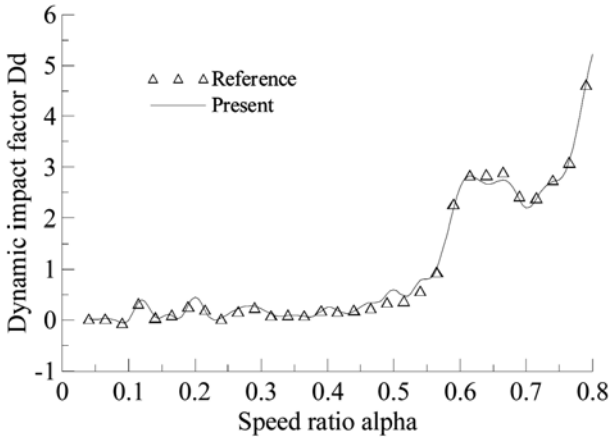

Figure 4. Dynamic impact factor for a 100-m span (5@20) continuous beam bridge with 0% damping ratio and no track irregularities under a train with five cars.

quickly increases from α=0.35 to α=0.6, then quickly decreases. For the continuous beam bridge, the impact increases quickly after α=0.48. When α is between 0.62 and 0.77, a plateau appears; the impact factor varies around 2.7 in this area. After this plateau, the impact factor increases again. This comparison shows that the dynamic behaviors of these two types of bridges are significantly different, although they share the same cross section and span length.

8.3. Example 3: A 32 m-48 m-32 m continuous box girder bridge under a Korea Train Express (KTX) train

To investigate the effects of bridge damping and track irregularity levels on the different bridge spans, a three-span continuous box girder bridge undergoing a KTX train is considered. The bridge spans consist of a widely used span combination of 32 m-48 m-32 m. The cross section of the bridge is shown in Fig. 5. The bridge is divided into 70 equal length beam elements; it is supported by abutments at the first and 71st nodes and by piers at the 21st and 51st nodes, respectively. The one-foot sprung masses are located at the positions of the 46 wheel sets of the KTX train, as shown in Fig. 6. The properties of the bridge and train are described in Table 4. Different levels of track irregularities are considered. The generated N_k random phase angles, θ_k, remain constant at all track levels; thus, the only effective parameter in track irregularities is the roughness coefficient, A.

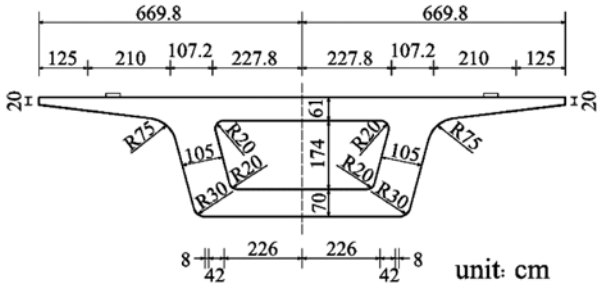

Figure 5. Cross section of the three-span continuous beam bridge in Example 3.

There are three parameter variations in this example: train speed, bridge damping ratio, and level of track irregularities. The train speed varies from 200 to 400 km/h, which is the normal operating range for high-speed trains. The bridge damping ratio is set into three conditions: no damping (ζ=0%), normal damping (ζ=2%), and high damping (ζ=4%). Four track irregularity conditions are considered: no track irregularities (smooth) and level 4, 5, and 6 track irregularities.

The dynamic response of the bridge is evaluated in two

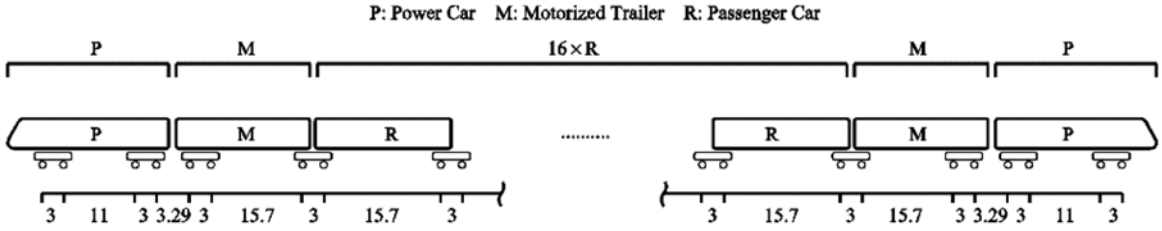

Figure 6. Wheel set arrangement of KTX train.

Table 4. Bridge and train properties in Example 3

L_b (m)	$\overline{m}$ (kg/m)	I (m^4)	E (MPa)	N_m	N_v
32+48+32	34666	16.24	34500	70	46
m_w (kg)	m_v (kg)	k_t (N/m)	c_t (Ns/m)	ζ	
3400	13600	9.12×10^6	8.6×10^4	0%, 2%, 4%	

Table 5. Maximum midspan static deformations for three-span continuous bridge in Example 3

Left span		Central span		Right span	
downward	upward	downward	upward	downward	upward
-0.601 mm	0.401 mm	-1.400 mm	0.327 mm	-0.601 mm	0.401 mm

ways. The first method is the dynamic impact factor (DIF), both upward and downward at the midpoint of each span. The static maximum upward and downward deformations of the midpoint of each span, listed in Table 5, are calculated through the moving static load test. This test set the train as a series of static concentrated forces placed on the bridge and changed the positions of these forces each time by a small distance. Figures 7, 8, and 9 show the DIFs of the left, central, and right spans, respectively, of the three-span continuous beam bridge under different conditions. Overall, the better track irregularity conditions and higher bridge damping ratios result in smaller bridge impact factors. However, the dynamic responses of different spans are very different. The resonance speed for the left span downward DIF is over 400 km/h, whereas those for the central and right spans are 260 and 300 km/h, respectively. For the upward DIF, the left span resonance speed is 260 km/h, whereas those of the central and right spans are 270 and 300 km/h, respectively. With the increased bridge damping ratio, the DIF at the local resonance speed range decreases significantly. For the non-resonance speed range, the track irregularities control the DIF; inferior track conditions produce much larger DIFs for all bridge spans.

The second way to evaluate the dynamic response of the bridge is the maximum rotation angle in both clockwise and counterclockwise directions at the ends of the spans. Figures 10, 11, 12, and 13 show the clockwise and counterclockwise maximum rotation angles of the bridge deck at the left abutment, the left pier, the right pier, and the right abutment, respectively. Overall, the bridge damping significantly reduced the local resonance of deck rotational displacements at four supports, but in most speed ranges, the track irregularities control the displacements and poorer track conditions result in larger rotation at the supports. The resonance speeds for the rotational displacements at the left abutment and the right abutment are similar to those for the DIFs at the midpoint of the left and right spans. The resonance speed for clockwise rotation at the left pier is approximately 260 km/h; that for the counter-clockwise direction is approximately 280 km/h. For the right pier, the resonance speed for clockwise rotation is approximately 300 km/h; that for the counterclockwise direction is approximately 280 km/h.

Because there are 46 one-foot sprung masses, the average maximum vertical acceleration of the upper sprung masses is calculated to evaluate the train body vibration, as shown in Fig. 14. The smaller vertical acceleration produces better driving comfort. When the track is perfectly smooth, the vertical acceleration of all train bodies is smaller than 0.34 m/s^2. When the track condition changes from smooth to rough, the dynamic responses of all train-bridge systems increase. However, the increase in the average acceleration of train bodies is much larger than the increase in the DIF of bridge spans or deck rotation angles at supports. When the train is running at approximately 300 km/h, the average vertical acceleration of the train bodies reaches its maximum value. Meanwhile, the bridge damping ratio has a low influence on the acceleration of the train body.

9. Conclusion

This study performed the dynamic analysis of a continuous beam bridge with different levels of track irregularities under a moving train. The system is simplified into a planar model. The bridge is regarded as an Euler-Bernoulli beam

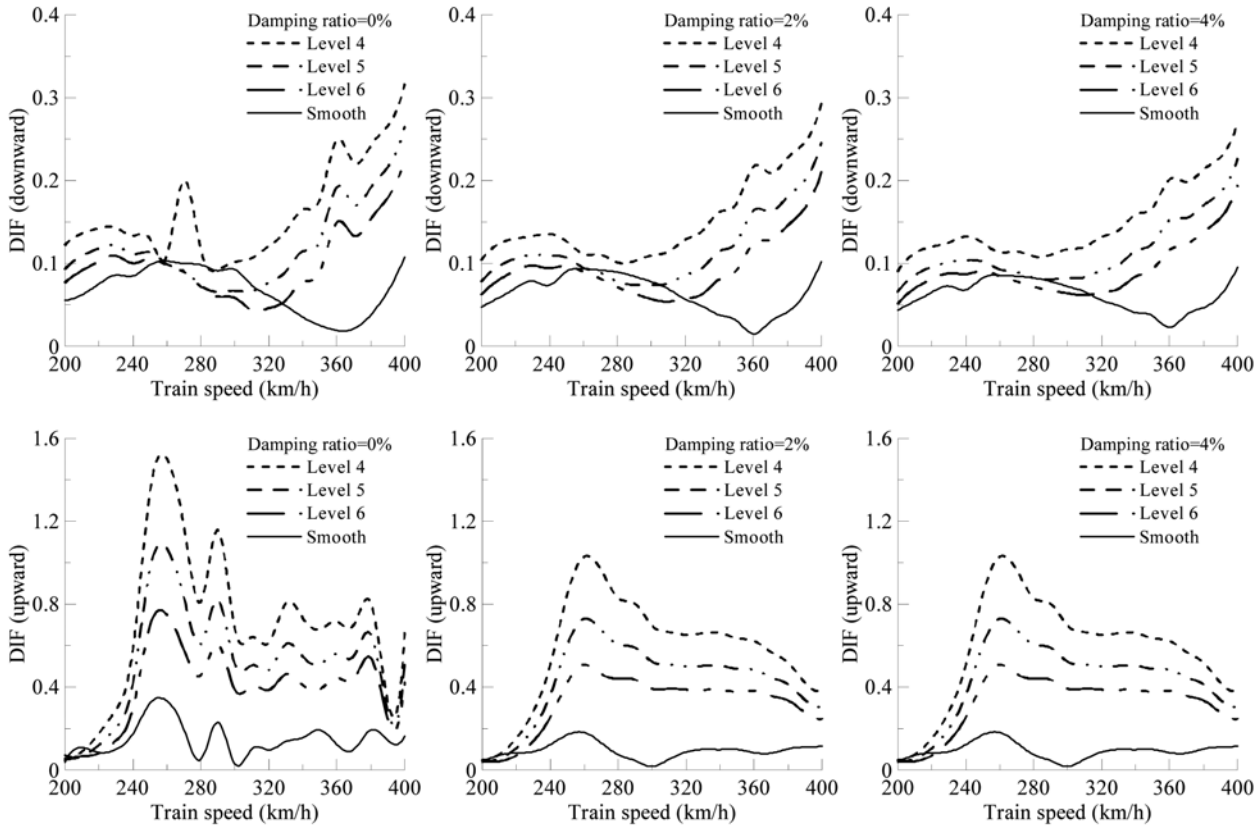

Figure 7. DIFs of the left span of a three-span continuous beam bridge under different conditions.

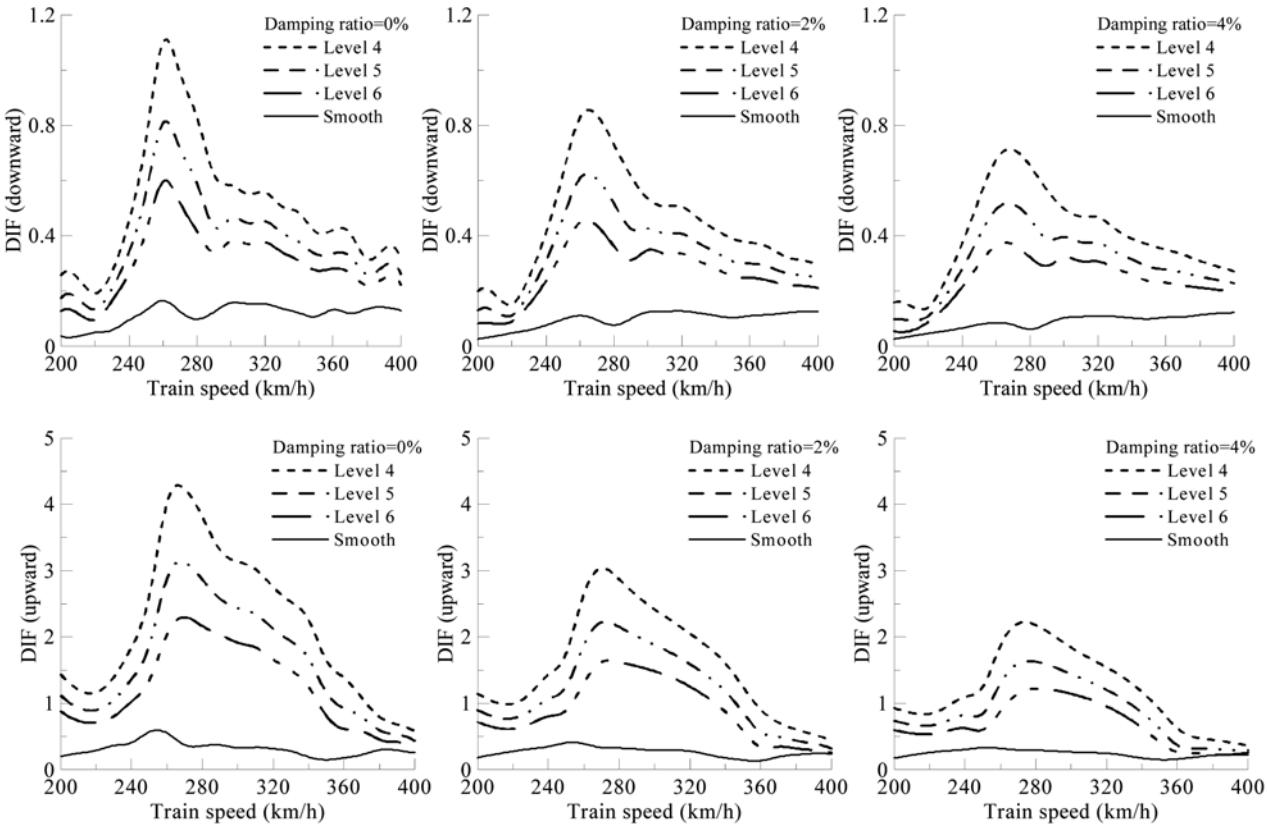

Figure 8. DIFs of the central span of a three-span continuous beam bridge under different conditions.

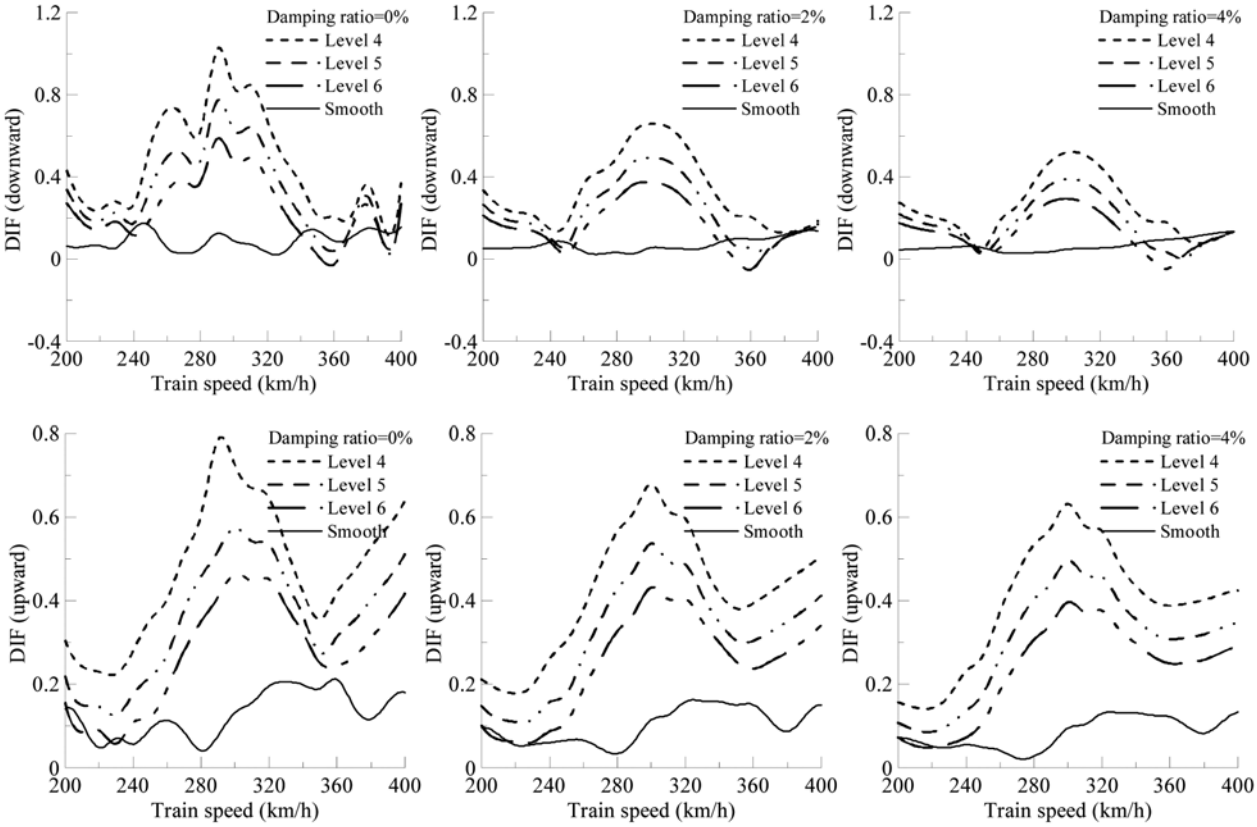

Figure 9. DIFs of the right span of a three-span continuous beam bridge under different conditions.

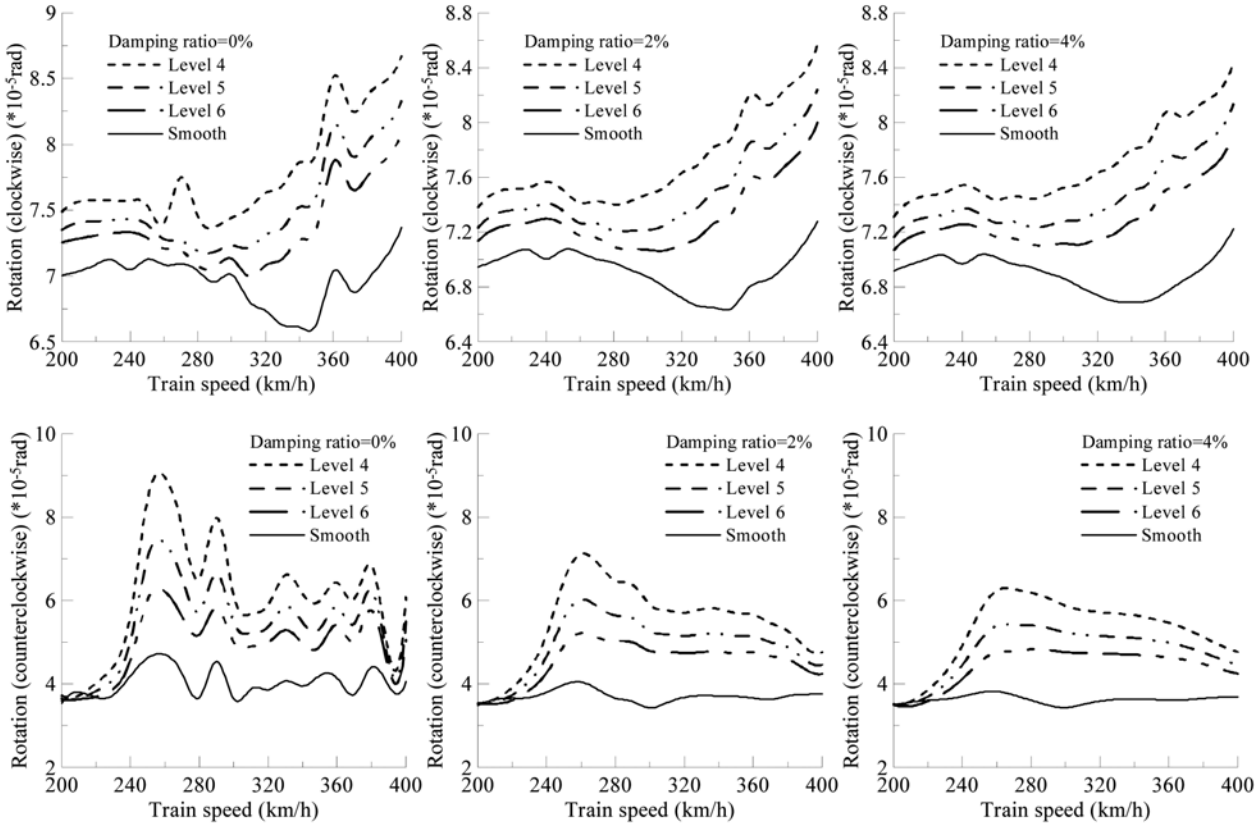

Figure 10. Maximum rotation at the left abutment of a three-span continuous beam bridge under different conditions.

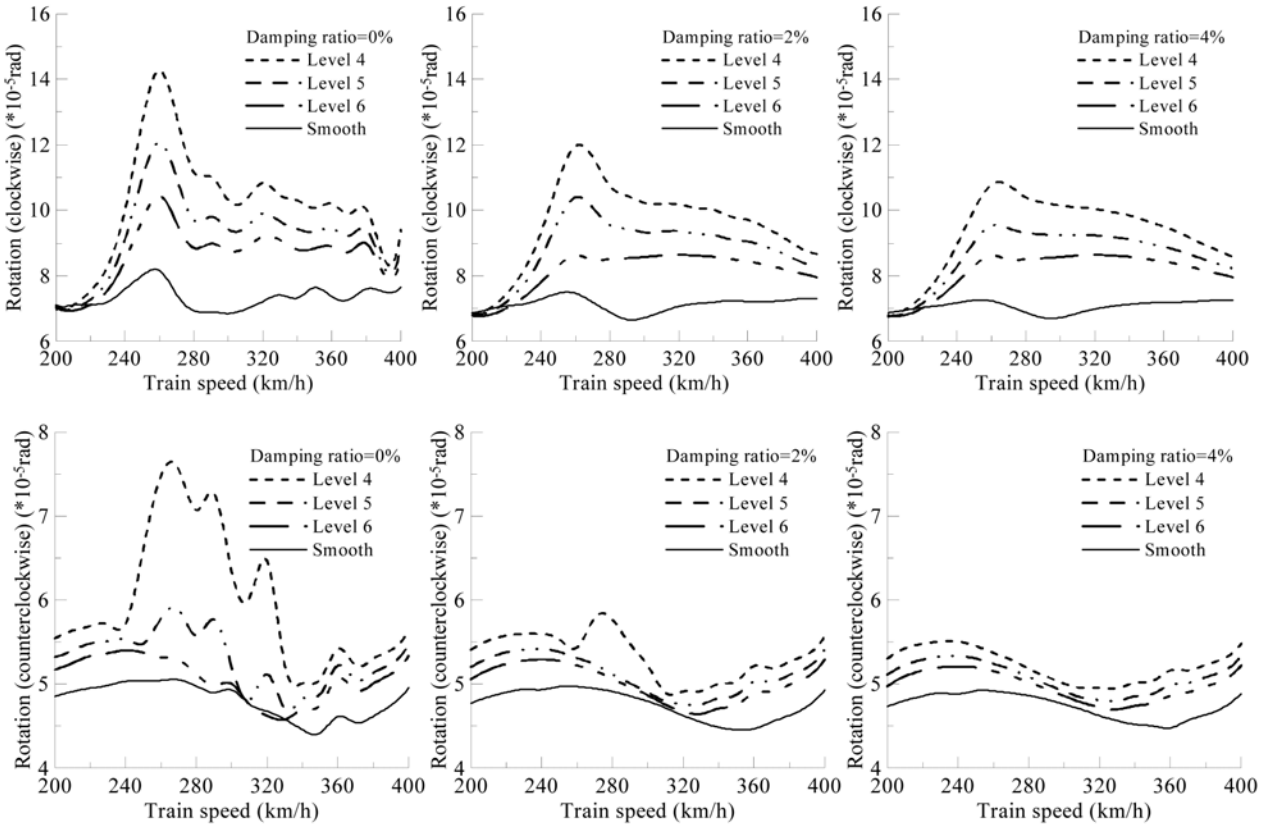

Figure 11. Maximum rotation at the left pier of a three-span continuous beam bridge under different conditions.

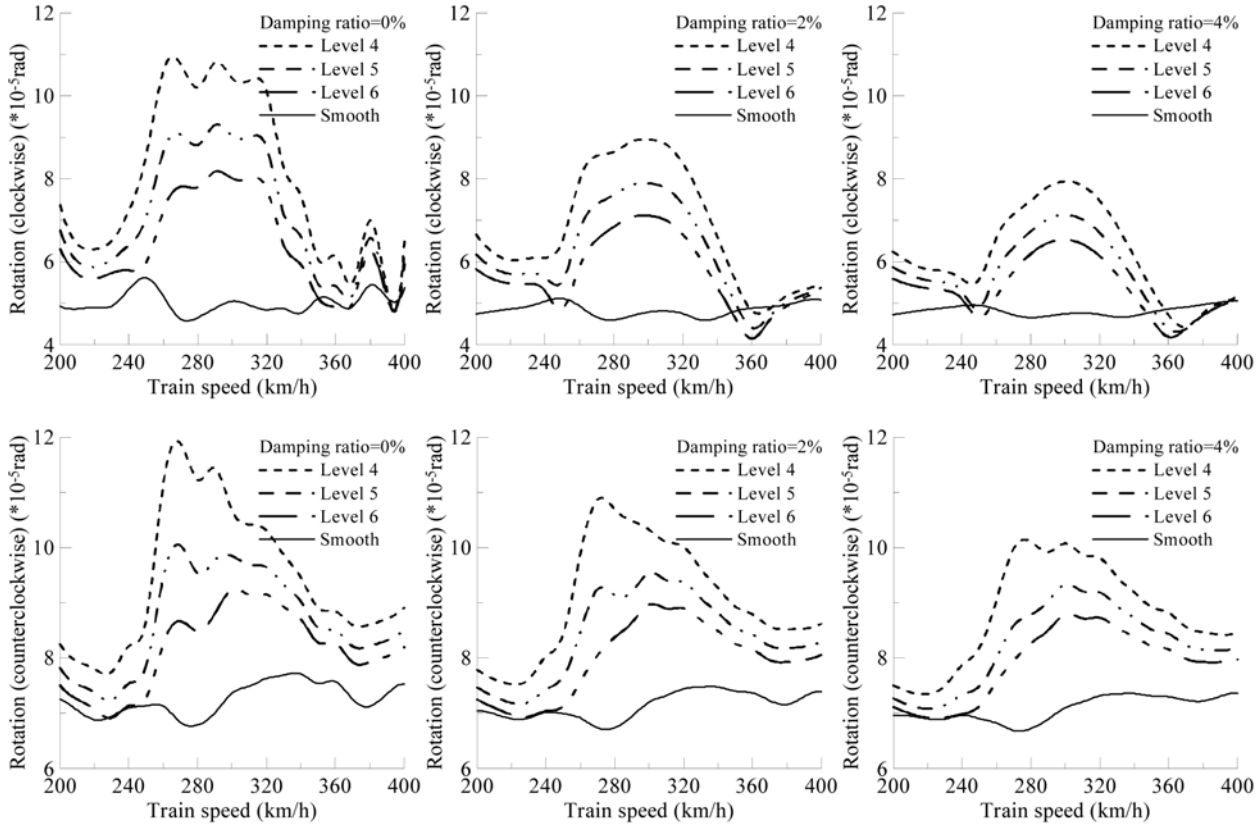

Figure 12. Maximum rotation at the right pier of a three-span continuous beam bridge under different conditions.

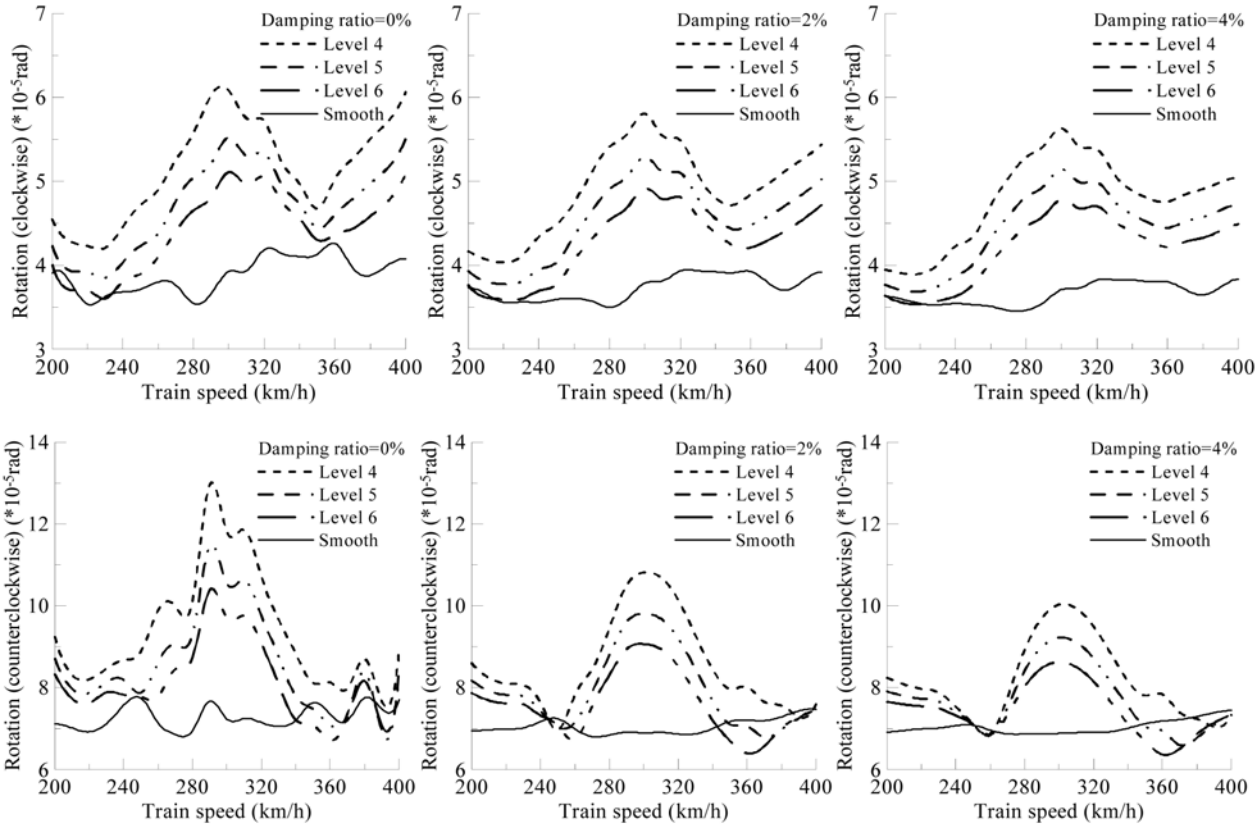

Figure 13. Maximum rotation at the right abutment of a three-span continuous beam bridge under different conditions.

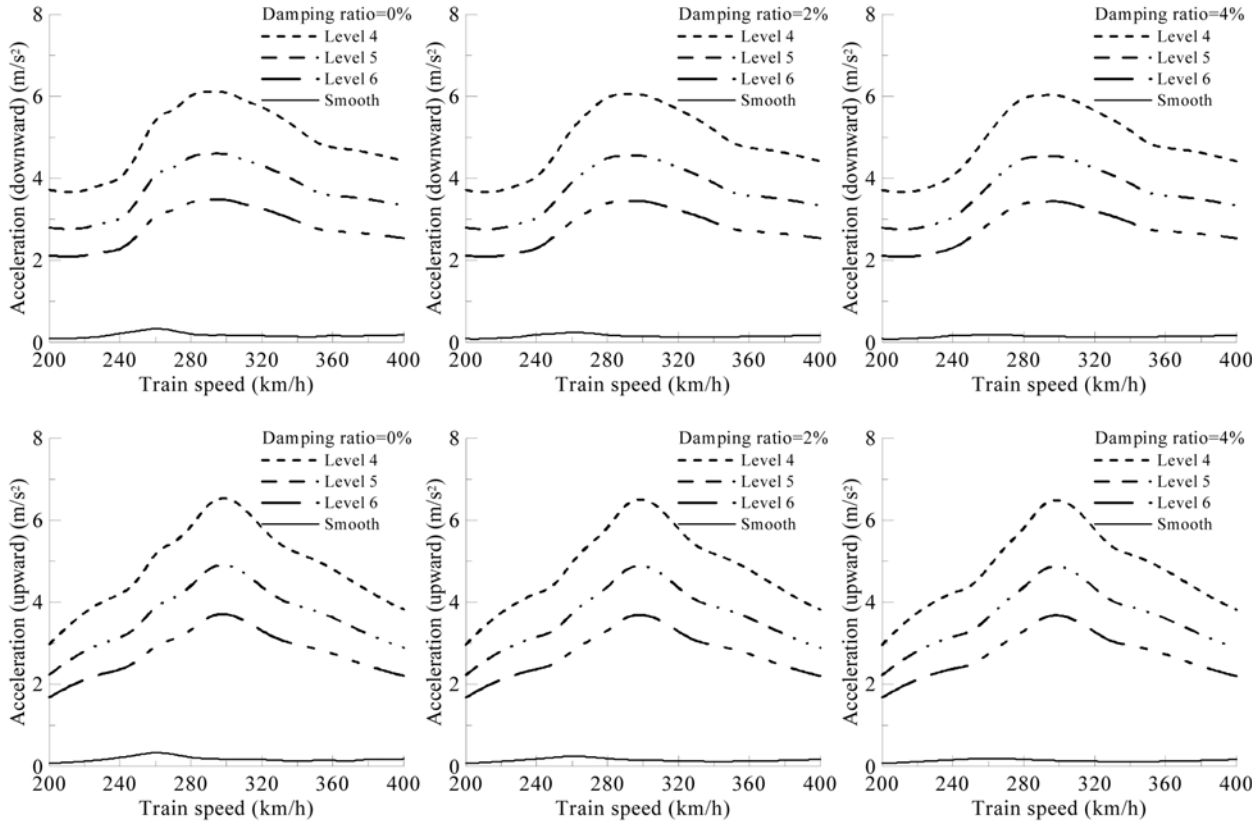

Figure 14. Average maximum vertical acceleration of all car bodies under different conditions.

supported by hinged supports, whereas the train is modeled as a series of one-foot sprung masses. The track irregularities are generated by PSD functions and distinguished into six different levels. The dynamic equations of motion for the train and the bridge are derived with the finite-element method. Through the shape constraints and contact force between the train and bridge, their equations of motion are coupled into the interaction equation of motion and solved by the Newmark-beta method combined with the Newton-Raphson method.

The calculated results are verified through comparisons with other researchers' results on the midpoint DIFs of a single-span simply supported bridge and a five-span continuous beam bridge under the same five-car train. To investigate the effects of train speed, bridge damping, and levels of track irregularities, the KTX train model and a 32 m-48 m-32 m continuous beam bridge is taken as an example. The following conclusions can be reached from this study:

(1) The bridge impact factors calculated in the verification examples agree well with other researchers' results. Comparing the two verification examples shows that the dynamic response of a continuous beam bridge is very different from that of a simply supported bridge. The resonance train speed range for a continuous beam bridge is higher than that of a simply supported bridge with the same cross section and span properties.

(2) Although the bridge span is symmetrical, the three spans have their own dynamic behavior and different resonance speeds. The rotational displacements at the supports are also mutually independent. Unlike the simply supported bridge, the upward displacement of the continuous beam bridge spans and deck rotation at the supports causes significant negative moment to the deck, which may result in cracking and other damage to the upper part of the deck. When designing a bridge, the amounts and positions of prepressed reinforcements in the deck can affect the dynamic analysis results for the bridge.

(3) Better track irregularities result in better performance of the system. In most speed ranges, track roughness is the primary cause of additional vibration of the train and bridge. Bridge damping can significantly reduce the resonance vibration of the bridge; however, it has almost no effect on reducing the maximum vertical acceleration of the train body.

Acknowledgments

This research was supported by the Basic Science Research Program through the National Research Foundation of Korea (NRF) funded by the Ministry of Education, Science and Technology (NRF-2012R1A1A 2007054). The authors wish to express their gratitude for this financial support.

References

Akin, J. and Mofid, M. (1989). "Numerical solution for response of beams with moving mass." *Journal of Structural Engineering*, 115(1), pp. 120-131.

Au, F.-T.-K., Wang, J.-J., and Cheung, Y.-K. (2002). "Impact study of cable-stayed railway bridges with random rail irregularities." *Engineering Structures*, 24(5), pp. 529-541.

Cheng, Y.-S., Au, F.-T.-K., and Cheung, Y.-K. (2001). "Vibration of railway bridges under a moving train by using bridge-track-vehicle element." *Engineering Structures*, 23(12), pp. 1597-1606.

Cheung, Y.-K., Au, F.-T.-K., Zheng, D.-Y., and Cheng, Y.-S. (1999). "Vibration of multi-span non-uniform bridges under moving vehicles and trains by using modified beam vibration functions." *Journal of Sound and Vibration*, 228(3), pp. 611-628.

Chu, K., Garg, V., and Wang, T. (1986). "Impact in railway prestressed concrete bridges." *Journal of Structural Engineering*, 112(5), pp. 1036-1051.

Dehestani, M., Mofid, M., and Vafai, A. (2009). "Investigation of critical influential speed for moving mass problems on beams." *Applied Mathematical Modelling*, 33(10), pp. 3885-3895.

Fryba, L. (2001). "A rough assessment of railway bridges for high speed trains." *Engineering Structures*, 23(5), pp. 548-556.

Hamid, A. and Yang, T.-L. (1982). *Analytical descriptions of track-geometry variations*. Transportation Research Board, pp. 19-26.

Johansson, C., Pacoste, C., and Karoumi, R. (2013). "Closed-form solution for the mode superposition analysis of the vibration in multi-span beam bridges caused by concentrated moving loads." *Computers & Structures*, 119, pp. 85-94.

Kwark, J.-W., Choi, E.-S., Kim, Y.-J., Kim, B.-S., and Kim, S.-I. (2004). "Dynamic behavior of two-span continuous concrete bridges under moving high-speed train." *Computers & Structures*, 82(4-5), pp. 463-474.

Lacarbonara, W. and Colone, V. (2007). "Dynamic response of arch bridges traversed by high-speed trains." *Journal of Sound and Vibration*, 304(1-2), pp. 72-90.

Lu, Y., Mao, L., and Woodward, P. (2012). "Frequency characteristics of railway bridge response to moving trains with consideration of train mass." *Engineering Structures*, 42, pp. 9-22.

Majka, M. and Hartnett, M. (2008). "Effects of speed, load and damping on the dynamic response of railway bridges and vehicles." *Computers & Structures*, 86(6), pp. 556-572.

Mao, L. and Lu, Y. (2013). "Critical speed and resonance criteria of railway bridge response to moving trains." *Journal of Bridge Engineering*, 18(2), pp. 131-141.

Mazilu, T. (2013). "Instability of a train of oscillators moving along a beam on a viscoelastic foundation." *Journal of Sound and Vibration*, 332(19), pp. 4597-4619.

Nikkhoo, A., Rofooei, F. R., and Shadnam, M. R. (2007).

"Dynamic behavior and modal control of beams under moving mass." *Journal of Sound and Vibration*, 306(3-5), pp. 712-724.

Olsson, M. (1985). "Finite element, modal co-ordinate analysis of structures subjected to moving loads." *Journal of Sound and Vibration*, 99(1), pp. 1-12.

Shin, J.-R., An, Y.-K., Sohn, H., and Yun, C.-B. (2010). "Vibration reduction of high-speed railway bridges by adding size-adjusted vehicles." *Engineering Structures*, 32(9), pp. 2839-2849.

Stancioiu, D., Ouyang, H., Mottershead, J. E., and James, S. (2011). "Experimental investigations of a multi-span flexible structure subjected to moving masses." *Journal of Sound and Vibration*, 330(9), pp. 2004-2016.

Thambiratnam, D. and Zhuge, Y. (1996). "Dynamic analysis of beams on an elastic foundation subjected to moving loads." *Journal of Sound and Vibration*, 198(2), pp. 149-169.

Wang, Y.-M. (1998). "The dynamical analysis of a finite inextensible beam with an attached accelerating mass." *International Journal of Solids and Structures*, 35(9-10), pp. 831-854.

Wu, Y.-S. and Yang, Y.-B. (2003). "Steady-state response and riding comfort of trains moving over a series of simply supported bridges." *Engineering Structures*, 25(2), pp. 251-265.

Yang, Y.-B. and Lin, B.-H. (1995). "Vehicle-bridge interaction analysis by dynamic condensation method." *Journal of Structural Engineering*, 121(11), pp. 1636-1643.

Yang, Y.-B. and Yau, J.-D. (1997). "Vehicle-bridge interaction element for dynamic analysis." *Journal of Structural Engineering*, 123(11), pp. 1512-1518.

Yang, Y.-B., Yau, J.-D., and Hsu, L.-C. (1997). "Vibration of simple beams due to trains moving at high speeds." *Engineering Structures*, 19(11), pp. 936-944.